What chemical species are responsible for new particle formation and growth in the Netherlands? A hybrid positive matrix factorization (PMF) analysis using aerosol composition (ACSM) and size (SMPS)

Farhan R. Nursanto[1], Roy Meinen[2], Rupert Holzinger[2], Maarten C. Krol[1,2], Xinya Liu[3], Ulrike Dusek[3], Bas Henzing[4], Juliane L. Fry[1]

[1]Meteorology and Air Quality (MAQ), Environmental Sciences Group, Wageningen University and Research (WUR), Wageningen, 6708PB, the Netherlands
[2]Institute for Marine and Atmospheric Research Utrecht, Department of Physics, Utrecht University, Princetonplein 5, 3584CC, Utrecht, the Netherlands
[3]Centre for Isotope Research (CIO), Energy and Sustainability Research Institute Groningen (ESRIG), University of Groningen, Groningen 9747 AG, the Netherlands
[4]Netherlands Organisation for Applied Scientific Research (TNO), Princetonlaan 6, 3584 Utrecht, the Netherlands

Correspondence to: Juliane L. Fry (juliane.fry@wur.nl)

Abstract. Aerosol formation acts as a sink for gas-phase atmospheric species that controls their atmospheric lifetime and environmental effects. To investigate aerosol formation and evolution in the Netherlands, a hybrid positive matrix factorization (PMF) analysis has been conducted using observations from May, June, and September 2021 collected in a rural site of Cabauw in Central Netherlands. The hybrid input matrix consists of the full organic mass spectrum acquired from a time-of-flight aerosol chemical speciation monitor (ToF-ACSM), ACSM species concentrations, and binned particle size distribution concentrations from a scanning mobility particle sizer (SMPS). These hybrid PMF analyses discerned six factors that describe aerosol composition variations: four size-driven factors that are related to new particle formation and growth (F6, F5, F4, and F3), and two bulk factors driven by composition, not size (F2, F1). The smallest-diameter size factor (F6) contains ammonium sulfate and organics, and typically occurs during the daytime. Newly formed particles, represented by F6, are correlated with wind from the southwesterly-westerly, northerly, and easterly sectors that transport sulfur oxides (SO_x), ammonia (NH_3), and organic precursors to Cabauw. As the particles grow from F6 to F3, nitrate plays an increasing role, and the particle loading diurnal cycle shifts from daytime to a nighttime maximum. The inorganic ion balance and organics composition in the bulk atmosphere affects the chemical composition variation across factors and seasons. Changing ammonium-sulfate-nitrate equilibrium shifts inorganic species among factors, and greater organics availability makes secondary organic aerosol (SOA) more influential in summertime aerosol growth, principally due to volatility differences produced by seasonal variation in photooxidation and temperature.

Keywords: new particle formation (NPF), positive matrix factorization (PMF), particle size distribution, sulfate aerosol, nitrate aerosol, organic aerosol

1. Introduction

Atmospheric aerosols are solid or liquid particles suspended in the air that are formed from natural or anthropogenic sources (Haywood, 2016). To describe the aerosol particle size distribution, four modes are generally distinguished according to the particle diameter (D_p): nucleation mode ($D_p < 20$ nm), Aitken mode (20 nm $< D_p < 100$ nm), accumulation mode (100 nm $< D_p < 1000$ nm), and coarse mode ($D_p > 1$ μm) (Hussein et al., 2004). New particle formation (NPF) is identified by a rapid buildup of high atmospheric concentrations of aerosol particles in the nucleation mode. These particles subsequently grow into Aitken mode particles and further (Maso et al., 2005; Spracklen et al., 2010; Salimi et al., 2015; Kerminen et al., 2018; Lee et al., 2019).

Aerosols impact the Earth by absorbing and scattering solar and terrestrial radiation (Andreae and Crutzen, 1997; Grantz et al., 2003; Wong et al., 2017; Marrero-Ortiz et al., 2019), and indirectly by producing or modifying clouds (Lohmann and Feichter, 2005; Mahowald et al., 2011; Fan et al., 2018). NPF plays a prominent role in cloud formation by contributing to

45 over 50% of cloud condensation nuclei formation, which affects the lifetime and radiative properties of clouds (Bianchi et al., 2016; Gordon et al., 2016; Haywood, 2016; Dall'Osto et al., 2018; Lee et al., 2019). These phenomena affect the ecosystem physically by modifying radiation diffusion, temperature, and precipitation (Grantz et al., 2003; Haywood, 2016; Lee et al., 2019). Aerosols also influence the ecosystem chemically through influencing the spatial patterns of nitrogen deposition (van der Swaluw et al., 2011; Wamelink et al., 2013) and oxidative processes (Xing et al., 2017), leading to ecological harm such

50 as soil pollution, water acidification, eutrophication, and loss of biodiversity (Erisman et al., 2011; Wamelink et al., 2013). In terms of public health, aerosols exhibit adverse effects on human health due to their size and chemical composition. NPF events are typically followed by air quality degradation, which is consistently associated with elevated pulmonary and cardiovascular morbidity and mortality worldwide (Ayala et al., 2012; Pope et al., 2020).

55 Sulfuric acid (H_2SO_4) is typically understood to be the most prevalent nucleation-inducing agent in NPF events, together with other airborne chemical species, including nitrate, bases (e.g., amines), and organic acids (Zhang et al., 2012; Kulmala et al., 2013; Zhang et al., 2015; Wagner et al., 2017; Lehtipalo et al., 2018; Kürten, 2019; Lee et al., 2019; Brean et al., 2021; Olin et al., 2022). Numerous studies also report low-volatility organic species, such as terpene oxidation products and organic nitrates, participating in the formation of new particles (Berkemeier et al., 2016; Bianchi et al., 2016; Tröstl et al., 2016;

60 Barsanti et al., 2017; Dall'Osto et al., 2018; Kerminen et al., 2018; Lee et al., 2019; Heinritzi et al., 2020).

In this work, we show that co-located measurements of aerosols' atmospheric composition and particle size distribution can be used to characterize the chemical composition of new particle and aerosol components that facilitate their growth. A time-of-flight aerosol chemical speciation monitor (ToF-ACSM, Aerodyne Inc.) allows the continuous and real-time quantification of

65 non-refractory chemical species in ambient air (Ng et al., 2011; Fröhlich et al., 2013). For particle size distributions, the scanning mobility particle sizer (SMPS) provides real-time measurement of submicron particle number concentrations of different sizes (Amaral et al., 2015; Wiedensohler et al., 2018).

Aerosol mass spectrometry measurements have been used extensively with positive matrix factorization (PMF) as a strategy

70 for aerosol source apportionment, especially regarding the organic components (Lanz et al., 2007; Jimenez et al., 2009; Ulbrich et al., 2009; Ng et al., 2010; Zhang et al., 2011). This paper combines the full organic mass spectrum and chemical species concentrations from ToF-ACSM with particle size distribution from SMPS into a hybrid PMF input matrix, to study the association between chemical composition and particle size distribution. A similar approach for hybrid ACSM-SMPS PMF analysis was used for a European aerosol dataset comparison (Dall'Osto et al., 2018). Previous studies on aerosol source

75 apportionment in the Netherlands have focused on organic aerosol composition (Mooibroek et al., 2011; Mensah et al., 2012; Schlag et al., 2016). Here, we analyze ACSM-SMPS datasets from Cabauw, the Netherlands, collected as part of the Ruisdael Observatory Land-Atmosphere Interactions Intensive Trace-gas and Aerosol (RITA) campaign in May to September 2021 (https://ruisdael-observatory.nl), using PMF to characterize the chemical species responsible for new particle formation and growth across several seasons. Several studies have shown NPF events dependent on air mass origin transporting different

80 pollutants (Hamed et al., 2007; Modini et al., 2009; Castro et al., 2010; Asmi et al., 2011; Németh and Salma, 2014; Nieminen et al., 2014; Qi et al., 2015; Mordas et al., 2016; Kolesar et al., 2017; Peng et al., 2017; Kerminen et al., 2018; Pushpawela et al., 2019), and therefore we also explore relationships between wind direction, wind speed, and factor timeseries to interpret source apportionment.

2. Methods and Instrumentation

2.1. Cabauw site and meteorological conditions

Measurements were performed at the CESAR tower (51.970° N, 4.926° E), managed and operated by the Royal Netherlands Meteorological Institute (KNMI, the Netherlands) (see Fig. 1). The tower is located near Cabauw, in the province of Utrecht, the Netherlands, approximately 18 km southwest of Utrecht city center, 31 km east of the city and (largest in Europe) port of Rotterdam, 45 km south of Amsterdam, and about 45 km southeast of the Dutch North Sea coast. To the east and south of the site are the provinces of Gelderland and Noord-Brabant, which consist mainly of forests, agricultural lands with clay and sand soil types for crops, and animal farms, specifically chicken and pig farms in the south and cattle in the east (CBS, 2022). The Cabauw site itself is rural and surrounded by agricultural lands. The dataset used in this analysis contains overlapping ACSM and SMPS data split into periods from 11–31 May 2021, 1–22 June 2021, and 1–30 September 2021, providing some seasonal variation. To simplify, we will refer to these periods as May, June, and September, respectively, in this paper.

Figure 1. Map of a part of the Netherlands showing the locations of the measurement stations Cabauw (main site) and Zegveld-Oude Meije (NH₃ measurements). The province, sea, and neighbouring country names are indicated in italic and light grey. The big cities of Amsterdam, The Hague, Rotterdam, and Utrecht in the area collectively known as "Randstad" are situated in Noord-Holland, Zuid-Holland, and Utrecht provinces. The urban and harbor area of Rotterdam extends as Europoort-Maasvlakte to the mouth of the Maas River.

In general, May 2021 was characterized by moderate spring temperatures with scattered precipitation transitioning into the warmer summer period. June 2021 had the highest temperatures and was the sunniest of the three periods, reflecting summer weather. September 2021 showed warm temperatures, with less radiation and precipitation compared to May 2021. Winds from south to southwest sector (180° to 225°) dominated in spring (May), bringing plumes from the agriculture-heavy province of Noord-Brabant. In summer (June), the prevailing air masses were coming from west-northwest to north-northeast (292.5° to 22.5°), bringing air from the North Sea and some major cities along the coast and/or in the Randstad, such as Rotterdam, The Hague, Amsterdam, and Utrecht. More diverse wind plumes were observed in September, ranging from easterly (22.5° to 112.5°), coming from the forested nature and agricultural areas in the province of Gelderland, and southerly (180° to 202.5°), coming from the province of Noord-Brabant. The meteorological variables for each period are summarized in Table 1 and the wind variables are visualized as wind roses in Fig. 2.

Table 1. Meteorological conditions on three periods analyzed (May, June, and September 2021). The periods represent spring, summer, and autumn weather respectively.

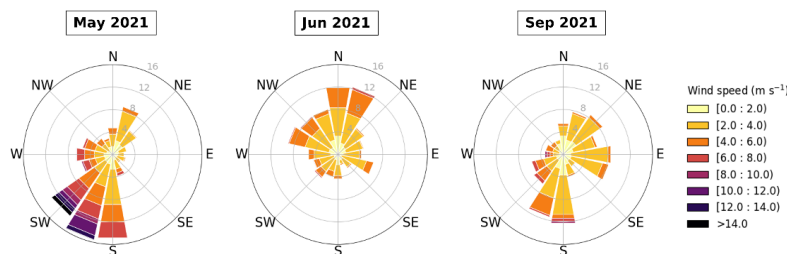| Period	Temperature (ºC)	Downward shortwave radiation (W m^{-2})	Precipitation (mm)
11–31 May 2021	11.8 (mean) 3.5 (low), 23.0 (high)	211.7 (mean) 1032.2 (max)	96.6 (total)
1–22 Jun 2021	18.7 (mean) 8.1 (low), 29.6 (high)	264.9 (mean) 957.2 (max)	31.2 (total)
1–30 Sep 2021	16.2 (mean) 5.7 (low), 26.7 (high)	142.0 (mean) 818.9 (max)	24.4 (total)

115

Figure 2. Wind rose plots for May, June, and September 2021. Winds from S up to SW sector were dominant in May. In June, the prevailing winds were from WNW up to the NNE sector. In September, two major wind directions were from the E and S sectors.

2.2. Measurements

120 The ToF-ACSM was the main instrument employed for this analysis. The instrument has been detailed in other work (Fröhlich et al., 2013). The ACSM was installed with an inlet at 5-meter height, a cyclone with size cut of 2.5 µm (PM$_{2.5}$), and an aerodynamic lens in the inlet system allowing the analysis of non-refractory organics, ammonium, nitrate, sulfate, chloride, and potassium in the aerosol phase. The instrument is equipped with a capture vaporizer (CV) instead of the standard vaporizer (SV), which is designed to increase the collection efficiency (Middlebrook et al., 2012; Jayne and Worsnop, 2016). By having

125 a narrow entrance, the CV increases the particle collision events and thus increases the contact with the hot vaporizer surface, minimizing particles that bounce without evaporation (Hu et al., 2017). Consequently, however, the fragmentation patterns are shifted towards smaller ion masses due to the additional thermal decomposition (Hu et al., 2017; Zheng et al., 2020). The ToF-ACSM provides unit mass resolution (UMR) mass spectra which are analyzed using Tofware v3.2 in Igor Pro 8. The fractions of measured UMR signals were assigned to individual aerosol species using the fragmentation table. On-site calibrations are

130 performed to determine the ionization efficiencies of the chemical species. The calibration with ammonium nitrate and ammonium sulfate gives ionization efficiency (IE) value of 250.0 ions pg^{-1} for nitrate (NO$_3$), and relative ionization efficiency (RIE) values of 1.40, 1.67, 1.30, 3.35, and 1.00 for organics, sulfate (SO$_4$), chloride (Cl), ammonium (NH$_4$), and potassium (K), respectively.

135 In addition to the aerosol measurements by the ToF-ACSM, ambient sulfur dioxide (SO$_2$) concentrations were obtained from the open-source data of Landelijk Meetnet Luchtkwaliteit (LML, https://www.luchtmeetnet.nl), measured at the same location. Ammonia (NH$_3$) concentrations were obtained from measurements in Zegveld-Oude Meije station, 20 km to the north of Cabauw station (see Fig. 1), also acquired from LML. The particle size distribution concentration measurements were conducted using a TROPOS-SMPS with 8 nm to 800 nm size range and 5-minute time resolution from a 5-meter height inlet.

140 The co-located weather data were retrieved from the Royal Netherlands Meteorological Institute (KNMI, https://www.knmi.nl).

2.3. Positive matrix factorization (PMF)

The 10-minute average matrices of organic fragment mass spectra were combined with the species average mass concentrations (i.e., organics (Org), ammonium (NH$_4$), nitrate (NO$_3$), sulfate (SO$_4$), chloride (Cl), and potassium (K)) and the 10-minute

145 average particle number concentrations (dN) in 18 particle diameter (D$_p$) size bins to generate hybrid input data matrices for

PMF analysis. Each organic fragment mass-to-ratio (m/z), species concentration, and size-binned particle concentration is treated as an individual variable in the PMF. The mass concentration variable values and errors were generated by Tofware v3.2. The particle size dataset from the SMPS instrument as categorized into 18 size bin variables (8–10 nm; 10–13 nm; 13–16 nm; 16–20 nm; 20-25 nm; 25–32 nm; 32–40 nm; 40–51 nm; 51–65 nm; 65–83 nm; 83–107 nm; 107–140 nm; 140–185 nm; 185–249 nm; 249–342 nm; 342–481 nm; 481–691 nm; and 691–853 nm). Each size bin contains the sum of four concentration points, averaged to 10 minutes. We use larger bin sizes for the larger diameters because larger particles occur less frequently. The errors for each size bin are taken to be the population standard deviation of the raw data. The variable values of species mass concentrations and particle number concentrations were weighted prior to analysis to ensure that individual peaks have similar magnitude as the organic mass spectrum. This weighting was done to give all variables the same importance in the PMF analysis.

We performed the analysis using the PMF Evaluation Tool (PET) v3.08 (Ulbrich et al., 2009) in Igor Pro 8. The details of applying positive matrix factorization (PMF) to aerosol mass spectrometry datasets have been discussed elsewhere in detail (Paatero and Tapper, 1994; Paatero, 1999; Ulbrich et al., 2009). The first step of the factor analysis was identifying the optimum number of factors by running unconstrained experiments using 2 to 10 factors. The optimum number of factors is selected by considering the lowest residuals of the PMF solutions, and whether all the factors are environmentally reasonable and unique based on their chemical composition. For all three-month datasets, this analysis converges to an optimum of 6 factors. The ordering of the factors is not identical across months and for ease of presentation, we reorder them so that factors of similar identity have the same factor number across months. The percent of signal explained by each factor is presented alongside plots of the factor profiles, to enable the reader to deduce the original factor ordering. The resulting hybrid PMF solution matrix is split back up into organic mass spectrum, species mass concentrations, and particle number concentration bin matrices, and the value of each variable is readjusted (undoing the previously described re-weighting) so that the ACSM species mass concentrations can still be interpreted quantitatively.

2.4. Wind analysis

To analyze the factors using wind variables, we investigate the prevailing wind for several pollution episodes observed in the dataset. Bivariate polar plots are generated for selected factor reconstructed mass concentration derived from PMF analyses and mass concentration for each ACSM species in each period using the "Openair" package in the "R" environment (Carslaw and Ropkins, 2012). The wind parameters are obtained from co-located measurement of 10-meter wind direction data acquired from KNMI.

3. Results and Discussion

3.1. Identification of PMF factors

3.1.1. Factor particle size distributions and composition

From the unconstrained experiments, the best PMF solution was found with six factors for the combined ACSM-SMPS matrix in each of the datasets for May 2021 (Fig. 3), June 2021 (Fig. S1), and September 2021 (Fig. S2), with similarities observed across months. As each period encompasses around one month of time series data, the factors discerned by the hybrid PMF analyses show typical average aerosol composition during each period, rather than individual pollution episode profiles that may vary over time.

Four factors have particle size profiles distributed in specific diameter subranges, which we interpret as related to new particle formation and growth. We therefore call these factors "size-driven". The size-driven factors resolved from the analysis possess

some similarities in composition across months, from ammonium sulfate-rich aerosol (F6) to varying mixture of organic aerosol (OA) and inorganic aerosol (IA) (F5, F4, and F3) (see Fig. 4). We interpret the smallest-diameter size-driven factor as a nucleation-mode factor (F6), which then grows with different composition, on average progressing from F6 to F3. The two bulk composition-driven factors are distributed across particle sizes, consisting of: (F2), an OA and IA mixed factor with a variable composition, and (F1), an organic aerosol factor with occasional traces of ammonium sulfate aerosol.

3.1.2. Factor organic profiles

The organic mass spectrum of each factor profile can be used to obtain information regarding the oxidation level of the factor. Oxidized organic compounds are characterized by a relatively high m/z 44 (f_{44}) signal, originating primarily from CO_2^+ fragments of carboxylic groups in organic compounds produced by thermal decomposition inside the ACSM vaporizer (Alfarra et al., 2004). This f_{44} fragment is often related to a high degree of oxidation and photochemical ageing (Alfarra et al., 2004; Ng et al., 2010). The m/z 43 (f_{43}) fragment is characteristic for both oxidized organic compounds (CH_3CO^+) and saturated hydrocarbon compounds ($C_3H_7^+$). Thus, factors with higher f_{44} and lower f_{43} values are understood to be more oxidized and are often classified as an oxygenated organic aerosol (OOA). Meanwhile, lower f_{44} and higher f_{43} values implies that the factor is less oxidized and is often labelled hydrocarbon-like organic aerosol (HOA). In this paper, we use these values only to compare the oxidation level between aerosol factors. It is also important to note that the ACSM used in this paper has a CV instead of a SV inlet (see **Sect. 2.2**), which is known to produce higher f_{44} values due to enhanced thermal decomposition (Hu et al., 2017), and therefore cannot be directly compared to PMF organic profiles in other works.
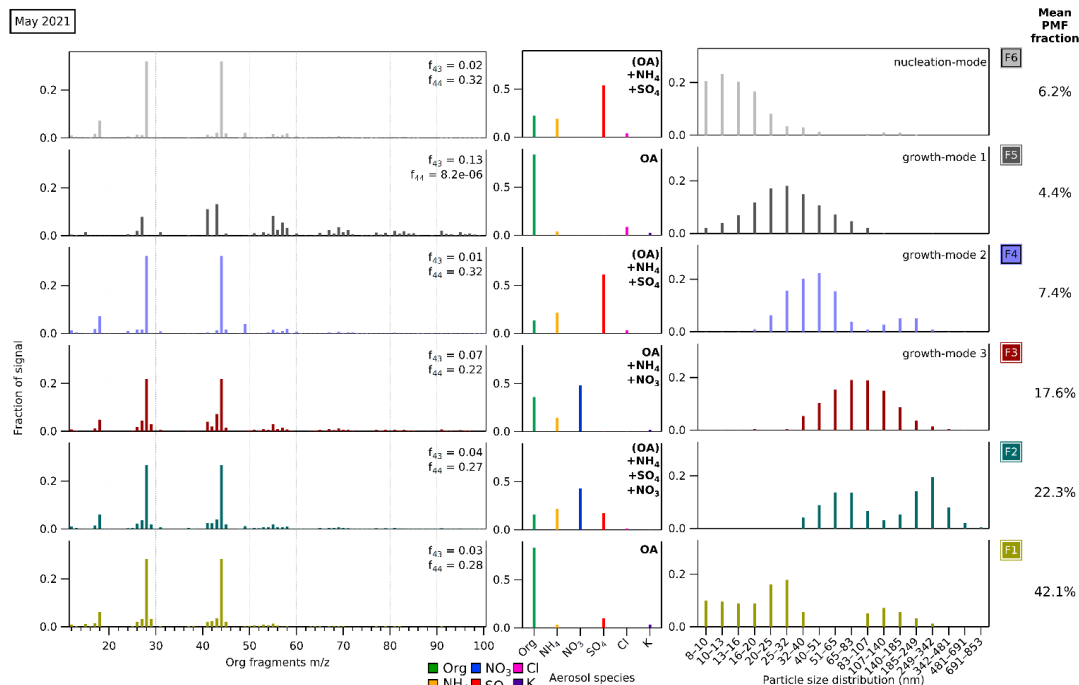

Figure 3. The profiles of 6-factor solution from the combined ACSM-SMPS dataset in May 2021. Each factor is split into three matrices with their own signal fraction axes. The lefthand panel shows the organic fragment mass spectrum profiles from ACSM. The values of f_{44} (CO_2^+ fragment) representing higher oxidation level and f_{43} (CH_3CO^+ and $C_3H_7^+$) representing lower oxidation level are given. The middle panel shows the ACSM standard aerosol species concentrations (organics (Org), ammonium (NH_4), nitrate (NO_3), sulfate (SO_4), chloride (Cl), and potassium (K)). The righthand panel shows the particle size distribution profiles from the SMPS. The mean PMF fractions are shown to the right, indicating the mean contribution of each hybrid PMF factor to the "total variable reconstruction" by PMF throughout the period (note we have reordered factors to be consistent across the 3 months). The factors in May 2021 are assigned as: (F1) OA, (F2) (OA)+NH_4+SO_4+NO_3, (F3) growth-mode 3 OA+NH_4+NO_3, (F4) growth-mode 2 (OA)+NH_4+SO_4, (F5) growth-mode 1 OA, and (F6)

nucleation-mode (OA)+NH$_4$+SO$_4$. Factors with OA listed inside parentheses indicates OA below 25% of the total mass. Similar figures for June and September 2021 can be found in Fig. S1 and Fig. S2.
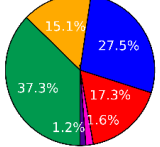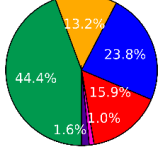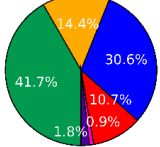
215

3.2. Bulk atmospheric chemical composition across periods

We hypothesize that the bulk atmospheric chemical composition influences how the chemical species are distributed across the PMF factors. The three periods have different average chemical composition as detected by the ToF-ACSM measurements. The mean concentrations of atmospheric species and the species percentages in the bulk atmosphere are summarized in Table

220 S1. For this assessment, we are using three mean concentration ratios summarized in Table 2 to characterize average composition. Ion balance ratio ($n_{NH_4}/(n_{NO_3}+2\times n_{SO_4}+n_{Cl})$) is the ratio between the measured ammonium (n_{NH_4}) and the total ammonium required to neutralize the major anions ($n_{NO_3}+2\times n_{SO_4}+n_{Cl}$). It illustrates the excess of atmospheric ammonium (cation), or nitrate (anion), and other possibilities based on aerosol chemistry (see Sect. S2 for details). This ion balance ratio was found to be unity in May (suggesting charge-balanced condition), less than unity in June (suggesting nitrate excess), and

225 more than unity in September (suggesting ammonium excess). We also examine the mean sulfate-to-nitrate molar concentration ratio (n_{SO_4}/n_{NO_3}), determining a sulfate-rich or sulfate-poor condition relatively. The mean organic-to-ammonium mass ratio (m_{Org}/m_{NH_4}) is used to show whether a period is organic-rich relative to other periods.

We have three different composition regimes measured during the three periods based on these ratios. In springtime (May),

230 we can see a sulfate-rich and nitrate-excess regime. In summertime (June), we have an organic-rich, sulfate-rich with nitrate-excess regime. Lastly, a sulfate-poor and ammonium-excess regime is observed in autumn (September). Below, we will discuss how these regimes influence the chemical composition of factors that were obtained from PMF analyses.

Table 2. Mean bulk atmospheric chemical composition in the three periods, summarized as the values of ion balance ratio
235 ($n_{NH_4}/(n_{NO_3}+2\times n_{SO_4}+n_{Cl})$) from linear regression, mean sulfate-to-nitrate ratio (n_{SO_4}/n_{NO_3}), and mean organic-to-ammonium ratio (m_{Org}/m_{NH_4}). The concentrations were detected by the ToF-ACSM in Cabauw. A more detailed information can be seen in Table S1.

Mean ratio	May 2021 (spring)	Jun 2021 (summer)	Sep 2021 (autumn)
Bulk aerosol composition* ■ Org ■ SO$_4$ ■ NH$_4$ ■ Cl ■ NO$_3$ ■ K	 15.1% 27.5% 37.3% 17.3% 1.2% 1.6%	 13.2% 23.8% 44.4% 15.9% 1.6% 1.0%	 14.4% 30.6% 41.7% 10.7% 1.8% 0.9%
$n_{NH_4}/(n_{NO_3}+2\times n_{SO_4}+n_{Cl})$**	0.99	0.98	1.08
n_{SO_4}/n_{NO_3}**	0.41	0.43	0.23
m_{Org}/m_{NH_4}*	2.47	3.36	2.90
Composition regime	sulfate-rich	nitrate excess, organic- and sulfate-rich	ammonium excess, sulfate-poor

*mass concentration, **molar concentration

3.3. Size-driven factors (F7, F6, F5, and F4)

Using the hybrid ACSM-SMPS datasets, four size-driven factors emerge from the PMF analyses as F6, F5, F4, and F3 (see
240 Fig. 3, Fig. S1, and Fig. S2). These factors are considered "size-driven" due to the approximately normally distributed particle concentrations in a specific sub-range of diameter. The four factors display different particle size clusters increasing in diameter from F6 to F3. The size-driven factors have diverse composition characterized by a variety of OA and IA mixtures, as can be seen in Fig. 4, discussed in more detail below.
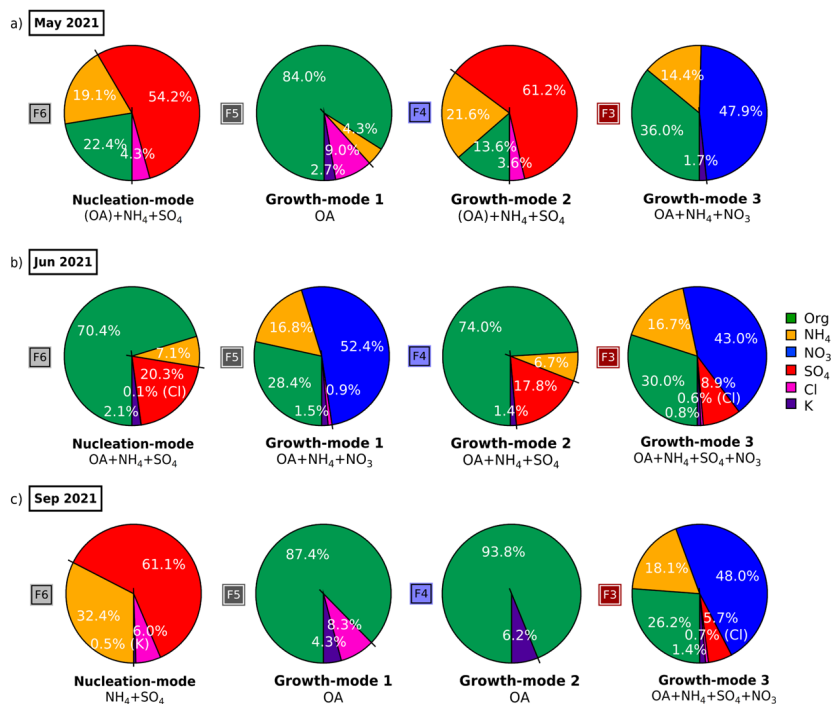
Figure 4. Pie charts showing mass percentage of each aerosol species contributing to each size-driven factor profile in (a) May 2021, (b) June 2021, and (c) September 2021. Green represents organics (Org), orange represents ammonium (NH_4), dark blue represents nitrate (NO_3), dark red represents sulfate (SO_4), pink represents chloride (Cl), and purple represents potassium (K). Factors with OA listed inside parentheses indicates OA below 25% of the total mass.

New particle formation (NPF) events are characterized by the rapidly increasing particle number concentration below 20 nm followed by particle growth, creating nearly vertical aligned peaks in particle number concentration plotted against time (Heintzenberg et al., 2007; Kerminen et al., 2018). In Fig. 5 and Fig. S3, we observe that the episodes during which the smallest size-driven factor (F6) fraction increases occur when the total aerosol mass concentration is relatively low. If we zoom into the timeseries, the NPF growth shapes appear during episodes that are dominated by the smallest size factor, F6 (see Fig. S4). The trace inorganic ions (chloride and potassium) in the factors are found to be correlated with the existence of sulfate and organic species, respectively, hinting at possible correlations with sea spray and biomass burning aerosol, respectively (see details in Sect. S4).
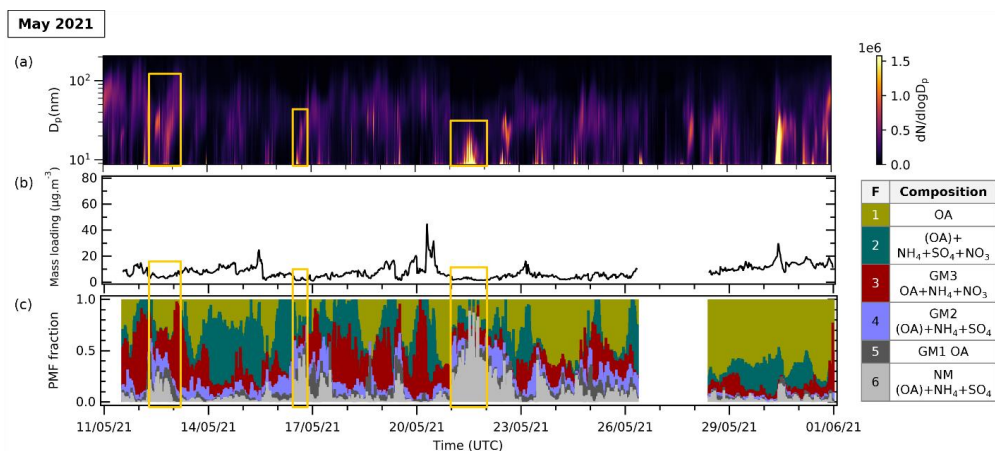
Figure 5. Time series of (a) particle size distribution ($dN/dlogD_p$) in cm^{-3} with logarithmic scale in particle size obtained from SMPS measurements, (b) total mass loading calculated from ACSM species concentration (using Tofware) in µg m^{-3}, and (c) reconstructed PMF fraction (stacked) from analysis in May 2021. Orange outlined sections indicate periods during which high episodes of size-driven factors are observed. These episodes coincide with relatively low total aerosol mass conditions and high fine particle concentrations. Similar figures for June and September 2021 can be found in Fig. S3.

3.3.1. F6: nucleation-mode factor

F6 correspond to particles in the nucleation mode growing into Aitken mode size range ($8 < D_p < 65$ nm). The size range differs slightly across months but is always the smallest particle size range among factors, which we therefore designate as nucleation mode. In all periods, F6 has ammonium sulfate as a major component. The factor further consists of ammonium (7.1% to 32.4%), sulfate (20.3% to 61.6%), organic compounds (0.0% to 70.4%), and traces of chloride (0.1% to 6.0%) and potassium (0.0% to 2.1%).

The mass percentage share between ammonium, sulfate, and organics of F6 depend on the composition regime in each period (see Fig. 4). The sulfate-rich regime with low bulk organics in springtime (May) leads to F6 being largely ammonium and sulfate (19.1% and 54.2%, respectively), followed by OA (22.4%) and chloride (4.8%). The organic-rich and sulfate-rich regime in summer (June) results in F6 being dominated by OA (70.4%) rather than ammonium and sulfate (7.1% and 20.3%, respectively), with traces of chloride (0.1%) and potassium (2.1%). In autumn (September), the ammonium-excess and sulfate-poor regime with low bulk organics results in the F6 composition being exclusively ammonium and sulfate (32.4% and 61.1%, respectively), with traces of chloride (6.0%) and potassium (0.5%). We interpret these results to mean that sulfate is a key component of condensation nuclei during NPF events, regardless of the bulk atmospheric composition. When the bulk organic concentration is high, it participates in particle nucleation. With excess ambient ammonium, however, particle condensation can occur without organic compounds.

Oxidation levels further explain the OA contribution difference in nucleation-mode particles. We can observe this variation by looking at the organic fragment spectrum of F6. High f_{44} value is observed in F6 where OA participates in new particle condensation during spring (May, $f_{44} = 0.32$) and summer (June, $f_{44} = 0.33$). In these months, higher mean radiation promotes photooxidation of organic vapors and semi-volatile oxidized organic compounds condense rapidly onto newly formed particles, resulting in higher OA contribution to nucleation-mode particles. In September, when mean radiation is lower, OA does not appear in F6. The organic mass spectra are consistent with this lower degree of oxidation, with lower f_{44} and high f_{43} value in autumn (September, $f_{44} = 5.8 \times 10^{-6}$ and $f_{43} = 0.16$).

We infer that only lower volatility, oxidized organic compounds can condense on freshly nucleated particles. The organic-rich regime combined with higher mean temperature favors the abundant condensation of available semi-volatile OA onto newly formed particles. Consistent with these results, several aerosol chamber experiments have reported that highly oxygenated-organic molecules (HOM) from biogenic and anthropogenic organic precursors play a dominant role in new particle formation and growth (Schobesberger et al., 2013; Ehn et al., 2014; Riccobono et al., 2014; Tröstl et al., 2016; Pospisilova et al., 2020; Zhao et al., 2021).

3.3.2. F5 to F3: growth-mode factors

F5, F4, and F3 are characterized by clustered particle sizes in the Aitken and accumulation mode region ($20 < D_p < 691$ nm). The size range differs across period but has particle size progressively growing from F5 to F3, which we thus designate the "growth-mode" factors. The growth-mode factors contain different composition across seasons, depending on the available semivolatile species for condensation.

In springtime (May), less-volatile and less-oxidized organic compounds ($f_{44} = 8.2 \times 10^{-6}$ and $f_{43} = 0.13$) condense onto newly formed particles, increasing the organic contribution in F5. The increase of OA in F5 is also observed for autumn (September), although in the case more highly oxidized organic compounds ($f_{44} = 0.21$ and $f_{43} = 0.07$) condense onto new particles. We suggest that although oxidized organic compounds are not involved in early particle condensation when the mean radiation is lower, they are incorporated in later growth. For spring and autumn, F5 consists of largely OA composition (84.0% to 87.4%), ammonium (4.3% only in May), chloride (8.3% to 9.0%), and potassium (2.7% to 4.3%).

In summertime (June), there is a substantial amount of nitrate (52.4%) in F5 alongside less oxygenated OA (28.4%, $f_{44} = 2.8 \times 10^{-8}$ and $f_{43} = 0.17$), ammonium (16.8%), chloride (0.9%), and potassium (1.5%). The ion balance ratio in June was less than unity, which can be due to excess nitrate aerosol (see Sect. S2). We propose that it indicates the promotion of semi-volatile organic nitrate formation in the summertime, condensing onto the newly formed particles as the temperature lowers. Organic nitrate comes from reaction between NO_x with less oxygenated organic compounds and condensing into aerosol phase more easily in this period. Further, we infer the possibility of biogenic source of the organic compounds involved in this organic nitrate source, due to the fact that we observe this composition only in the hottest and sunniest month of June and less oxygenated.

As particles grow into the larger size ranges F4 and F3, they incorporate more OA and ammonium salts. F4 resembles the composition of either the two smallest size-driven factors (F6 or F5), which may be due to continuation of smaller particle growth with the same composition. F3, the largest particle size range among size-driven factors, contains nitrate as the main component (43.0% to 48.0%) followed by OA (26.2% to 36.0%), and ammonium (14.4% to 18.1%). The dominant contribution of nitrate is observed across periods regardless of the nitrate composition regime. Overall, the composition of these size-driven factors suggests that, while sulfate is key to nucleation, nitrate plays a more important role in particle growth, which is related to the ammonium-sulfate-nitrate aerosol chemistry (see Sect. S2).

3.3.3. Relationships with mean radiation and temperatures

The reconstructed PMF masses show the influence of mean downward shortwave radiation and temperature on NPF events. The average PMF mass fraction of nucleation-mode particles (F6) is higher in summertime (June) compared to other periods (see Fig. S1) due to higher mean radiation and temperatures (see Table 1). In summer (June), F6 accounts in average 22.3%

of total reconstructed PMF mass while in spring (May) and summer (September), they only represent 6.2% and 4.1%, respectively. The more frequent appearance of NPF growth events during summer can be seen in Fig. S3a. The occurrence of

335   NPF events is generally favored in high radiation (Modini et al., 2009; Peltola et al., 2022) and warmer temperatures (Jokinen et al., 2022; Peltola et al., 2022). Solar radiation provides the UV radiation that promotes photochemical reactions and turbulent motions needed to form new particles (Wehner et al., 2015; Dada et al., 2017; Kerminen et al., 2018; Sellegri et al., 2019).

The diurnal cycles of the size-driven factors shown in Fig. 6 (May) and Fig. S5 (June and September) also shows the influence

340   of shortwave radiation and temperature on particle formation. Going from F6 to F3, we observe that the factors' diurnal pattern tends to shift from a daytime peak (F6 peaks in the middle of the day) to higher nighttime concentration as the particle size grows. Regional-scale NPF normally takes place during the daytime between sunrise and sunset, where it can carry on for several hours (Hamed et al., 2007; Hussein et al., 2009; Németh and Salma, 2014; Qi et al., 2015; Dai et al., 2017; Kerminen et al., 2018; Kalkavouras et al., 2020), although there are also instances of NPF happening during the night in various locations

345   (Hirsikko et al., 2012; Vehkamäki and Riipinen, 2012; Rose et al., 2018; Kammer et al., 2018) or quiet NPF during non-event days (Kulmala et al., 2012; Dada et al., 2018; Kulmala et al., 2022). Daytime peaks in F6 can be seen in spring (see Fig. 6) and summer (see Fig. S5) when the mean radiation is higher. This peak is less visible during autumn when mean radiation is lower (see Fig. S5). The sulfate-rich new particle factor F6 also appears around the same time as the precursor gas SO_2, with the most obvious match between SO_2 and the F6 diurnal cycle observed in spring (May, see Fig. 6).

350

Unlike the nucleation-mode F6, the growth-mode F5 and F4 have different diurnal patterns across periods, corresponding to their diverse compositions. F5 and F4 also exhibit consistently less diurnal variation, except for F5 during summer (see Fig. S5), when it tracks with the highest mean radiation across periods. In summertime (June), when there was more daylight and radiation available to promote NPF and growth, F5 has a pronounced peak in the afternoon, later than the F6 peak.

355

F3 shows more elevated nighttime concentrations across seasons (see Fig. 6 and Fig. S5). Lower nocturnal temperatures foster the condensation of semivolatile chemical species into the aerosol phase, increasing the nighttime particle concentration. The increase in the particle concentration during the night can also be facilitated by a shallower nocturnal boundary layer.
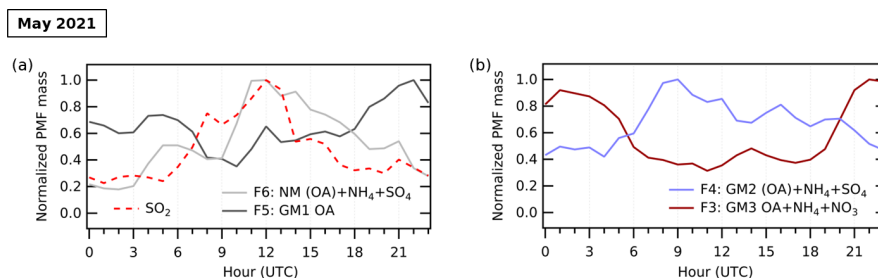

Figure 6. Normalized diurnal cycles in May 2021 of (a) the size-driven factors of F6 and F5, and SO_2 as the sulfate precursor, and (b) the size-driven factors of F4 and F3. Notice that from F4 to F3, the factors' diurnal pattern shifted from high daytime to high nighttime concentration. Similar figures for June and September 2021 can be found in Fig. S5.

3.3.4. Relationship of new particle formation with wind variables

365   To study the relationship between wind variables and new particle formation in Cabauw, we compare timeseries of wind variables and the reconstructed PMF fraction of the nucleation-mode (F6) and first growth-mode (F5) in Fig. 7 (May) and Fig. S6 (June and September). We observe that new particle formation episodes are correlated mainly with air masses transported from southwesterly-westerly sector or northerly-easterly sector. These wind sectors are the suppliers of organics, sulfate, ammonium, and their precursor gas that determine the main composition of F6 (see Fig. S7 and Fig. S8). Westerlies represent

370   a source of sulfate, which mainly comes from sulfur oxides (SO_x) emission along the waterway of Rotterdam's harbor, the busiest port in Europe. The sulfate in air transported to Cabauw from the northern to eastern sector may arise from SO_x precursor from other urban, shipping, industry centers (e.g., Amsterdam city and port, Utrecht city), and power plants to the site (see Fig. 1) (Henschel et al., 2013; Fioletov et al., 2016; Ledoux et al., 2018). The supply of ammonium for new particle condensation through NH_3 emission comes from the agricultural practices that take place around the Cabauw site, with

375   tendency of higher NH_3 and ammonium from the southern sector. The easterlies extending to north are sources of VOCs coming from the forested nature areas in the provinces Utrecht and Gelderland, which are subsequently transformed into SOA.

The different prevailing wind affects the F6 composition and frequency. In spring (May) and autumn (September), new particle formation mainly correlates with winds from southerly and westerly directions (see Fig. 2), and thus has less organic

380   composition. In summer (June), winds coming from the north or east contribute to NPF events (see Fig. 2), supplying more organics to the site. As previously discussed in Sect. 3.3.3, the abundant organics combined with higher radiation and temperatures allow semi-volatile oxidized organics to directly condense onto newly formed particles, increasing NPF events and F6 mass fraction during summer (see Fig. S6).
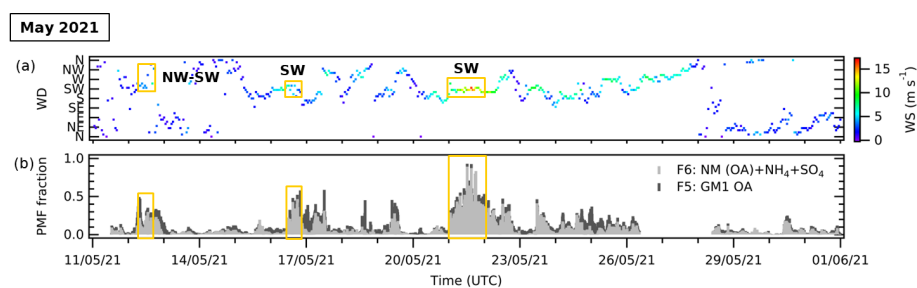
Figure 7. Timeseries of (a) wind direction (WD) color-coded with wind speed (WS), and (b) reconstructed PMF fractions F6 and F5 (stacked) corresponding to nucleation-mode and first growth-mode particles in May 2021. Orange outlined sections indicate high F6 and F5 episodes. We observe that new particle formation episodes are correlated with air masses from the southwesterly-westerly sector. Similar figures for June and September 2021 can be found in Fig. S6, showing more contributions from northerly-easterly wind directions.

385

390 **3.4. Bulk composition factors (F2 and F1)**

The two bulk composition factors yielded by the PMF analyses are F2 and F1 (see Fig. 3, Fig. S1, and Fig. S2). We call these factors bulk because they are composition-driven and found across the size distribution, rather than in a specific size range. They collectively account for a large fraction of total aerosol mass loading (31.1% to 64.4%).

395   F2 is characterized by the presence of a mixture of OA and IA. In Fig. S9, we can see that the diurnal cycle of F2 is similar to the diurnal pattern of total aerosol mass loading in spring (May). It is less similar in summer (June) and autumn (September) due to scarcity of OA mass, which is mainly found in the size-driven factors. This pattern suggests that F2 is the result of condensation of available semi-volatile chemical constituents over the course of the day.

400   F1 is composed mainly of OA with a trace amount of IA, containing the majority of OA in every month. The abundance of m/z 44 fragments indicates that factor F1 represents aged organic aerosol, resembling OA profiles observed at the same site in previous studies (Mensah et al., 2012; Paglione et al., 2014; Schlag et al., 2016). The factor is related to airmasses arriving from the easterly to southerly sector (see Fig. S10 in Sect. S3 for details). Considering the organic profile, the high mass loading percentage, and the source regions across periods, we attribute F1 to background regional and continental OA.

12

405   **4. Conclusions**

In this work, we have shown that hybrid ACSM-SMPS PMF analysis can be used to determine the chemical constituents associated with new particle formation and growth. The analyses of three selected periods enable us to use the seasonality of the factor profiles, representing conditions of spring (sunny and warm) for May, summer (very sunny and hot) for June, and autumn (less sunny and warm) for September, as well as different prevailing winds, to attribute factor sources. Different

410   chemical composition regimes were observed across these seasons, which manifested as differences in the species controlling aerosol growth.

New particle formation episodes appeared when the total aerosol concentration was low, with key contributions from ammonium sulfate, regardless of bulk aerosol composition regime. This new particle formation and growth exhibits a diurnal

415   pattern dominated by daytime formation that shifts to nighttime growth as the particle size increases. While sulfate promote new particle formation, nitrate is more influential in condensational growth. Organics participate in either new particle formation or growth.

The abundance of organics, sulfate, and ammonium aerosol, as well as the mean radiation and temperature, govern the chemical

420   species distribution across the factors. As a result, different modes of new particle formation and growth exist. The sulfate-rich regime in spring results in the nucleation-mode containing a mixture ammonium sulfate and organics. The organic-rich regime, higher mean radiation, and higher mean temperature in summer results in larger contribution of oxidized organic vapors in new particle formation. The ammonium-excess condition in autumn promotes nucleation without the presence of organic compounds.

425

A particle growth mode that arises from condensation of semi-volatile organics from the bulk atmospheric composition is observed in F5. In particular, the substantial contribution of nitrate in F5 during summer could be seen as the possible promotion of organic nitrate formation in nitrate excess condition in higher radiation, condensing during the particle growth when the temperature is lower. F4 is seen as the continuation of previous growth modes with similar composition but larger

430   particle size range. The factor with the largest particle diameter sub-range, F3, has a nitrate-rich composition across the seasons, illustrating the ubiquitous importance of nitrate.

New particle formation is most pronounced with winds from the southwest-west, or north and east. These directions supply precursors gases, with the westerlies bringing SO_x from the port of Rotterdam, southwesterlies bringing NH_3 from agricultural

435   emissions, and northerlies and easterlies bring organic vapors from the forest and nature areas. There is also an indication of SO_x sources from other urban centers to the north and east. The influence of the wind direction can be clearly seen during the summer, where instead of southern and western winds, the prevailing winds were from the north and east and brought abundant organics, resulting in the rapid growth of large amounts of OA.

440   In sum, this novel combination of composition and size information into the statistical PMF tool, combined with meteorological and gas-phase auxiliary data, provides a powerful tool to assess the factors that control aerosol production in a complex region, heavily influenced by agricultural and industrial activities, alongside biogenic emissions of VOCs.

Code availability

The analysis and graphics are mainly generated using Igor Pro 8. The code utilized in the PMF analysis is part of the PMF

445   Evaluation Tool (PET) v3.08 written as Igor procedures, available at https://cires1.colorado.edu/jimenez-

group/wiki/index.php/PMF-AMS_Analysis_Guide#PMF_Evaluation_Tool_Software (Ulbrich et al., 2009). The map, pollution roses, and particle size distribution time series are generated using Python 3.9 packages. The map is generated using "SciTools/cartopy v0.21.1" Python package, available at https://doi.org/10.5281/zenodo.7430317 (Elson et al., 2022). The pollution roses are generated using "windrose v1.8.1" Python package, available at https://doi.org/10.5281/zenodo.7465610

450 (Celles et al., 2022). The particle size distribution time series are plotted using open-source Python code written by Lee Tiszenkel, available at https://github.com/ltisz/Banana-Plot. The bivariate polar plots of concentrations are generated using "Openair" package in the "R" environment, available at https://davidcarslaw.github.io/openair/ (Carslaw and Ropkins, 2012).

Data availability

The ACSM-SMPS datasets were collected as part of the Ruisdael Observatory Land-Atmosphere Interactions Intensive Trace-

455 gas and Aerosol (RITA) campaign in May to September 2021 (https://ruisdael-observatory.nl) and available upon request. The gaseous phase species concentration can be retrieved from open-source data provided by Landelijk Meetnet Luchtkwaliteit (LML, https://www.luchtmeetnet.nl). The meteorological variables during the period are provided by the Royal Netherlands Meteorological Institute (KNMI, https://www.knmi.nl) and available upon request.

Author contributions

460 JLF and FRN designed the research; RM, RH, BH, and XL collected the data; FRN and JLF analyzed the data; FRN and JLF wrote the manuscript draft; MCK, RH, and UD reviewed and edited the manuscript.

Competing interests

The authors declare that they have no conflict of interest.

Acknowledgments

References

Alfarra, M. R., Coe, H., Allan, J. D., Bower, K. N., Boudries, H., Canagaratna, M. R., Jimenez, J. L., Jayne, J. T., Garforth, A. A., Li, S.-M., and Worsnop, D. R.: Characterization of urban and rural organic particulate in the Lower Fraser Valley using
470 two Aerodyne Aerosol Mass Spectrometers, Atmospheric Environment, 38, 5745–5758, https://doi.org/10.1016/j.atmosenv.2004.01.054, 2004.

Amaral, S., de Carvalho, J., Costa, M., and Pinheiro, C.: An Overview of Particulate Matter Measurement Instruments, Atmosphere, 6, 1327–1345, https://doi.org/10.3390/atmos6091327, 2015.

Andreae, M. O. and Crutzen, P. J.: Atmospheric Aerosols: Biogeochemical Sources and Role in Atmospheric Chemistry,
475 Science, 276, 1052–1058, https://doi.org/10.1126/science.276.5315.1052, 1997.

Ansari, A. S. and Pandis, S. N.: Response of Inorganic PM to Precursor Concentrations, Environ. Sci. Technol., 32, 2706–2714, https://doi.org/10.1021/es971130j, 1998.

Asmi, E., Kivekäs, N., Kerminen, V.-M., Komppula, M., Hyvärinen, A.-P., Hatakka, J., Viisanen, Y., and Lihavainen, H.: Secondary new particle formation in Northern Finland Pallas site between the years 2000 and 2010, Atmos. Chem. Phys., 11,
480 12959–12972, https://doi.org/10.5194/acp-11-12959-2011, 2011.

Ayala, A., Brauer, M., Mauderly, J. L., and Samet, J. M.: Air pollutants and sources associated with health effects, Air Qual Atmos Health, 5, 151–167, https://doi.org/10.1007/s11869-011-0155-2, 2012.

Barsanti, K. C., Kroll, J. H., and Thornton, J. A.: Formation of Low-Volatility Organic Compounds in the Atmosphere: Recent Advancements and Insights, J. Phys. Chem. Lett., 8, 1503–1511, https://doi.org/10.1021/acs.jpclett.6b02969, 2017.

485 Berkemeier, T., Ammann, M., Mentel, T. F., Pöschl, U., and Shiraiwa, M.: Organic Nitrate Contribution to New Particle Formation and Growth in Secondary Organic Aerosols from α-Pinene Ozonolysis, Environ. Sci. Technol., 50, 6334–6342, https://doi.org/10.1021/acs.est.6b00961, 2016.

Bianchi, F., Tröstl, J., Junninen, H., Frege, C., Henne, S., Hoyle, C. R., Molteni, U., Herrmann, E., Adamov, A., Bukowiecki, N., Chen, X., Duplissy, J., Gysel, M., Hutterli, M., Kangasluoma, J., Kontkanen, J., Kürten, A., Manninen, H. E., Münch, S.,
490 Peräkylä, O., Petäjä, T., Rondo, L., Williamson, C., Weingartner, E., Curtius, J., Worsnop, D. R., Kulmala, M., Dommen, J., and Baltensperger, U.: New particle formation in the free troposphere: A question of chemistry and timing, Science, 352, 1109–1112, https://doi.org/10.1126/science.aad5456, 2016.

Brean, J., Dall'Osto, M., Simó, R., Shi, Z., Beddows, D. C. S., and Harrison, R. M.: Open ocean and coastal new particle formation from sulfuric acid and amines around the Antarctic Peninsula, Nat. Geosci., 14, 383–388,
495 https://doi.org/10.1038/s41561-021-00751-y, 2021.

Carslaw, D. C. and Ropkins, K.: openair — An R package for air quality data analysis, Environmental Modelling & Software, 27–28, 52–61, https://doi.org/10.1016/j.envsoft.2011.09.008, 2012.

Castro, A., Alonso-Blanco, E., González-Colino, M., Calvo, A. I., Fernández-Raga, M., and Fraile, R.: Aerosol size distribution in precipitation events in León, Spain, Atmospheric Research, 96, 421–435, https://doi.org/10.1016/j.atmosres.2010.01.014,
500 2010.

CBS: Agriculture; crops, livestock and land use by general farm type, region, CBS, 2022.

Celles, S., Filipe, Quick, J., Samuël Weber/GwendalD, Kittner, J., Strawberry Beach Sandals, Ogasawara, I., Bachant, P., Maussion, F., Kvalsvik, J., R, M., Raj, S. P., McCann, J., and Sspagnol: python-windrose/windrose: v1.8.1, https://doi.org/10.5281/ZENODO.7465610, 2022.

505 Chen, G., Canonaco, F., Tobler, A., Aas, W., Alastuey, A., Allan, J., Atabakhsh, S., Aurela, M., Baltensperger, U., Bougiatioti, A., De Brito, J. F., Ceburnis, D., Chazeau, B., Chebaicheb, H., Daellenbach, K. R., Ehn, M., El Haddad, I., Eleftheriadis, K., Favez, O., Flentje, H., Font, A., Fossum, K., Freney, E., Gini, M., Green, D. C., Heikkinen, L., Herrmann, H., Kalogridis, A.-C., Keernik, H., Lhotka, R., Lin, C., Lunder, C., Maasikmets, M., Manousakas, M. I., Marchand, N., Marin, C., Marmureanu, L., Mihalopoulos, N., Močnik, G., Nęcki, J., O'Dowd, C., Ovadnevaite, J., Peter, T., Petit, J.-E., Pikridas, M., Matthew Platt,
510 S., Pokorná, P., Poulain, L., Priestman, M., Riffault, V., Rinaldi, M., Różański, K., Schwarz, J., Sciare, J., Simon, L., Skiba, A., Slowik, J. G., Sosedova, Y., Stavroulas, I., Styszko, K., Teinemaa, E., Timonen, H., Tremper, A., Vasilescu, J., Via, M., Vodička, P., Wiedensohler, A., Zografou, O., Cruz Minguillón, M., and Prévôt, A. S. H.: European aerosol phenomenology − 8: Harmonised source apportionment of organic aerosol using 22 Year-long ACSM/AMS datasets, Environment International, 166, 107325, https://doi.org/10.1016/j.envint.2022.107325, 2022.

515 Dada, L., Paasonen, P., Nieminen, T., Buenrostro Mazon, S., Kontkanen, J., Peräkylä, O., Lehtipalo, K., Hussein, T., Petäjä, T., Kerminen, V.-M., Bäck, J., and Kulmala, M.: Long-term analysis of clear-sky new particle formation events and nonevents in Hyytiälä, Atmos. Chem. Phys., 17, 6227–6241, https://doi.org/10.5194/acp-17-6227-2017, 2017.

Dada, L., Chellapermal, R., Buenrostro Mazon, S., Paasonen, P., Lampilahti, J., Manninen, H. E., Junninen, H., Petäjä, T., Kerminen, V.-M., and Kulmala, M.: Refined classification and characterization of atmospheric new-particle formation events
520 using air ions, Atmos. Chem. Phys., 18, 17883–17893, https://doi.org/10.5194/acp-18-17883-2018, 2018.

Dai, L., Wang, H., Zhou, L., An, J., Tang, L., Lu, C., Yan, W., Liu, R., Kong, S., Chen, M., Lee, S., and Yu, H.: Regional and local new particle formation events observed in the Yangtze River Delta region, China, J. Geophys. Res. Atmos., 122, 2389–2402, https://doi.org/10.1002/2016JD026030, 2017.

Dall'Osto, M., Beddows, D. C. S., Asmi, A., Poulain, L., Hao, L., Freney, E., Allan, J. D., Canagaratna, M., Crippa, M.,
525 Bianchi, F., de Leeuw, G., Eriksson, A., Swietlicki, E., Hansson, H. C., Henzing, J. S., Granier, C., Zemankova, K., Laj, P., Onasch, T., Prevot, A., Putaud, J. P., Sellegri, K., Vidal, M., Virtanen, A., Simo, R., Worsnop, D., O'Dowd, C., Kulmala, M., and Harrison, R. M.: Novel insights on new particle formation derived from a pan-european observing system, Sci Rep, 8, 1482, https://doi.org/10.1038/s41598-017-17343-9, 2018.

Docherty, K. S., Aiken, A. C., Huffman, J. A., Ulbrich, I. M., DeCarlo, P. F., Sueper, D., Worsnop, D. R., Snyder, D. C.,
530 Peltier, R. E., Weber, R. J., Grover, B. D., Eatough, D. J., Williams, B. J., Goldstein, A. H., Ziemann, P. J., and Jimenez, J. L.:

The 2005 Study of Organic Aerosols at Riverside (SOAR-1): instrumental intercomparisons and fine particle composition, Atmos. Chem. Phys., 11, 12387–12420, https://doi.org/10.5194/acp-11-12387-2011, 2011.

Ehn, M., Thornton, J. A., Kleist, E., Sipilä, M., Junninen, H., Pullinen, I., Springer, M., Rubach, F., Tillmann, R., Lee, B., Lopez-Hilfiker, F., Andres, S., Acir, I.-H., Rissanen, M., Jokinen, T., Schobesberger, S., Kangasluoma, J., Kontkanen, J.,
535   Nieminen, T., Kurtén, T., Nielsen, L. B., Jørgensen, S., Kjaergaard, H. G., Canagaratna, M., Maso, M. D., Berndt, T., Petäjä, T., Wahner, A., Kerminen, V.-M., Kulmala, M., Worsnop, D. R., Wildt, J., and Mentel, T. F.: A large source of low-volatility secondary organic aerosol, Nature, 506, 476–479, https://doi.org/10.1038/nature13032, 2014.

Elson, P., De Andrade, E. S., Lucas, G., May, R., Hattersley, R., Campbell, E., Dawson, A., Stephane Raynaud, Scmc72, Little, B., Snow, A. D., Donkers, K., Blay, B., Killick, P., Wilson, N., Peglar, P., Lbdreyer, Andrew, Szymaniak, J., Berchet,
540   A., Bosley, C., Davis, L., Filipe, Krasting, J., Bradbury, M., Kirkham, D., Stephenworsley, Clément, Caria, G., and Herzmann, D.: SciTools/cartopy: v0.21.1, , https://doi.org/10.5281/ZENODO.7430317, 2022.

Erisman, J. W., Galloway, J., Seitzinger, S., Bleeker, A., and Butterbach-Bahl, K.: Reactive nitrogen in the environment and its effect on climate change, Current Opinion in Environmental Sustainability, 3, 281–290, https://doi.org/10.1016/j.cosust.2011.08.012, 2011.

545   Fan, J., Rosenfeld, D., Zhang, Y., Giangrande, S. E., Li, Z., Machado, L. A. T., Martin, S. T., Yang, Y., Wang, J., Artaxo, P., Barbosa, H. M. J., Braga, R. C., Comstock, J. M., Feng, Z., Gao, W., Gomes, H. B., Mei, F., Pöhlker, C., Pöhlker, M. L., Pöschl, U., and de Souza, R. A. F.: Substantial convection and precipitation enhancements by ultrafineaerosol particles, Science, 359, 411–418, https://doi.org/10.1126/science.aan8461, 2018.

Farmer, D. K., Matsunaga, A., Docherty, K. S., Surratt, J. D., Seinfeld, J. H., Ziemann, P. J., and Jimenez, J. L.: Response of
550   an aerosol mass spectrometer to organonitrates and organosulfates and implications for atmospheric chemistry, Proc. Natl. Acad. Sci. U.S.A., 107, 6670–6675, https://doi.org/10.1073/pnas.0912340107, 2010.

Fioletov, V. E., McLinden, C. A., Krotkov, N., Li, C., Joiner, J., Theys, N., Carn, S., and Moran, M. D.: A global catalogue of large SO_2 sources and emissions derived from the Ozone Monitoring Instrument, Atmos. Chem. Phys., 16, 11497–11519, https://doi.org/10.5194/acp-16-11497-2016, 2016.

555   Fröhlich, R., Cubison, M. J., Slowik, J. G., Bukowiecki, N., Prévôt, A. S. H., Baltensperger, U., Schneider, J., Kimmel, J. R., Gonin, M., Rohner, U., Worsnop, D. R., and Jayne, J. T.: The ToF-ACSM: a portable aerosol chemical speciation monitor with TOFMS detection, Atmos. Meas. Tech., 6, 3225–3241, https://doi.org/10.5194/amt-6-3225-2013, 2013.

Gordon, H., Sengupta, K., Rap, A., Duplissy, J., Frege, C., Williamson, C., Heinritzi, M., Simon, M., Yan, C., Almeida, J., Tröstl, J., Nieminen, T., Ortega, I. K., Wagner, R., Dunne, E. M., Adamov, A., Amorim, A., Bernhammer, A.-K., Bianchi, F.,
560   Breitenlechner, M., Brilke, S., Chen, X., Craven, J. S., Dias, A., Ehrhart, S., Fischer, L., Flagan, R. C., Franchin, A., Fuchs, C., Guida, R., Hakala, J., Hoyle, C. R., Jokinen, T., Junninen, H., Kangasluoma, J., Kim, J., Kirkby, J., Krapf, M., Kürten, A., Laaksonen, A., Lehtipalo, K., Makhmutov, V., Mathot, S., Molteni, U., Monks, S. A., Onnela, A., Peräkylä, O., Piel, F., Petäjä, T., Praplan, A. P., Pringle, K. J., Richards, N. A. D., Rissanen, M. P., Rondo, L., Sarnela, N., Schobesberger, S., Scott, C. E., Seinfeld, J. H., Sharma, S., Sipilä, M., Steiner, G., Stozhkov, Y., Stratmann, F., Tomé, A., Virtanen, A., Vogel, A. L., Wagner,
565   A. C., Wagner, P. E., Weingartner, E., Wimmer, D., Winkler, P. M., Ye, P., Zhang, X., Hansel, A., Dommen, J., Donahue, N. M., Worsnop, D. R., Baltensperger, U., Kulmala, M., Curtius, J., and Carslaw, K. S.: Reduced anthropogenic aerosol radiative forcing caused by biogenic new particle formation, Proc. Natl. Acad. Sci. U.S.A., 113, 12053–12058, https://doi.org/10.1073/pnas.1602360113, 2016.

Grantz, D. A., Garner, J. H. B., and Johnson, D. W.: Ecological effects of particulate matter, Environment International, 29,
570   213–239, https://doi.org/10.1016/S0160-4120(02)00181-2, 2003.

Hamed, A., Joutsensaari, J., Mikkonen, S., Sogacheva, L., Dal Maso, M., Kulmala, M., Cavalli, F., Fuzzi, S., Facchini, M. C., Decesari, S., Mircea, M., Lehtinen, K. E. J., and Laaksonen, A.: Nucleation and growth of new particles in Po Valley, Italy, Atmos. Chem. Phys., 7, 355–376, https://doi.org/10.5194/acp-7-355-2007, 2007.

Haywood, J.: Atmospheric Aerosols and Their Role in Climate Change, in: Climate Change, Elsevier, 449–463,
575   https://doi.org/10.1016/B978-0-444-63524-2.00027-0, 2016.

Heinritzi, M., Dada, L., Simon, M., Stolzenburg, D., Wagner, A. C., Fischer, L., Ahonen, L. R., Amanatidis, S., Baalbaki, R., Baccarini, A., Bauer, P. S., Baumgartner, B., Bianchi, F., Brilke, S., Chen, D., Chiu, R., Dias, A., Dommen, J., Duplissy, J., Finkenzeller, H., Frege, C., Fuchs, C., Garmash, O., Gordon, H., Granzin, M., El Haddad, I., He, X., Helm, J., Hofbauer, V., Hoyle, C. R., Kangasluoma, J., Keber, T., Kim, C., Kürten, A., Lamkaddam, H., Laurila, T. M., Lampilahti, J., Lee, C. P.,
580   Lehtipalo, K., Leiminger, M., Mai, H., Makhmutov, V., Manninen, H. E., Marten, R., Mathot, S., Mauldin, R. L., Mentler, B., Molteni, U., Müller, T., Nie, W., Nieminen, T., Onnela, A., Partoll, E., Passananti, M., Petäjä, T., Pfeifer, J., Pospisilova, V., Quéléver, L. L. J., Rissanen, M. P., Rose, C., Schobesberger, S., Scholz, W., Scholze, K., Sipilä, M., Steiner, G., Stozhkov,

Y., Tauber, C., Tham, Y. J., Vazquez-Pufleau, M., Virtanen, A., Vogel, A. L., Volkamer, R., Wagner, R., Wang, M., Weitz,
L., Wimmer, D., Xiao, M., Yan, C., Ye, P., Zha, Q., Zhou, X., Amorim, A., Baltensperger, U., Hansel, A., Kulmala, M., Tomé,
585 A., Winkler, P. M., Worsnop, D. R., Donahue, N. M., Kirkby, J., and Curtius, J.: Molecular understanding of the suppression
of new-particle formation by isoprene, Atmos. Chem. Phys., 20, 11809–11821, https://doi.org/10.5194/acp-20-11809-2020,
2020.

Heintzenberg, J., Wehner, B., and Birmili, W.: How to find bananas in the atmospheric aerosol?: new approach for analyzing
atmospheric nucleation and growth events, Tellus B, 59, 273–282, https://doi.org/10.1111/j.1600-0889.2007.00249.x, 2007.

590 Henschel, S., Querol, X., Atkinson, R., Pandolfi, M., Zeka, A., Le Tertre, A., Analitis, A., Katsouyanni, K., Chanel, O., Pascal,
M., Bouland, C., Haluza, D., Medina, S., and Goodman, P. G.: Ambient air SO$_2$ patterns in 6 European cities, Atmospheric
Environment, 79, 236–247, https://doi.org/10.1016/j.atmosenv.2013.06.008, 2013.

Hirsikko, A., Vakkari, V., Tiitta, P., Manninen, H. E., Gagné, S., Laakso, H., Kulmala, M., Mirme, A., Mirme, S., Mabaso,
D., Beukes, J. P., and Laakso, L.: Characterisation of sub-micron particle number concentrations and formation events in the
595 western Bushveld Igneous Complex, South Africa, Atmos. Chem. Phys., 12, 3951–3967, https://doi.org/10.5194/acp-12-3951-
2012, 2012.

Hu, W., Campuzano-Jost, P., Day, D. A., Croteau, P., Canagaratna, M. R., Jayne, J. T., Worsnop, D. R., and Jimenez, J. L.:
Evaluation of the new capture vaporizer for aerosol mass spectrometers (AMS) through field studies of inorganic species,
Aerosol Science and Technology, 51, 735–754, https://doi.org/10.1080/02786826.2017.1296104, 2017.

600 Hussein, T., Puustinen, A., Aalto, P. P., Mäkelä, J. M., Hämeri, K., and Kulmala, M.: Urban aerosol number size distributions,
Atmos. Chem. Phys., 4, 391–411, https://doi.org/10.5194/acp-4-391-2004, 2004.

Hussein, T., Junninen, H., Tunved, P., Kristensson, A., Dal Maso, M., Riipinen, I., Aalto, P. P., Hansson, H.-C., Swietlicki,
E., and Kulmala, M.: Time span and spatial scale of regional new particle formation events over Finland and Southern Sweden,
Atmos. Chem. Phys., 9, 4699–4716, https://doi.org/10.5194/acp-9-4699-2009, 2009.

605 Jayne, J. T. and Worsnop, D. R.: Particle Capture Device, 2016.

Jimenez, J. L., Canagaratna, M. R., Donahue, N. M., Prevot, A. S. H., Zhang, Q., Kroll, J. H., DeCarlo, P. F., Allan, J. D., Coe,
H., Ng, N. L., Aiken, A. C., Docherty, K. S., Ulbrich, I. M., Grieshop, A. P., Robinson, A. L., Duplissy, J., Smith, J. D.,
Wilson, K. R., Lanz, V. A., Hueglin, C., Sun, Y. L., Tian, J., Laaksonen, A., Raatikainen, T., Rautiainen, J., Vaattovaara, P.,
Ehn, M., Kulmala, M., Tomlinson, J. M., Collins, D. R., Cubison, M. J., E., Dunlea, J., Huffman, J. A., Onasch, T. B., Alfarra,
610 M. R., Williams, P. I., Bower, K., Kondo, Y., Schneider, J., Drewnick, F., Borrmann, S., Weimer, S., Demerjian, K., Salcedo,
D., Cottrell, L., Griffin, R., Takami, A., Miyoshi, T., Hatakeyama, S., Shimono, A., Sun, J. Y., Zhang, Y. M., Dzepina, K.,
Kimmel, J. R., Sueper, D., Jayne, J. T., Herndon, S. C., Trimborn, A. M., Williams, L. R., Wood, E. C., Middlebrook, A. M.,
Kolb, C. E., Baltensperger, U., and Worsnop, D. R.: Evolution of Organic Aerosols in the Atmosphere, Science, 326, 1525–
1529, https://doi.org/10.1126/science.1180353, 2009.

615 Jokinen, T., Lehtipalo, K., Thakur, R. C., Ylivinkka, I., Neitola, K., Sarnela, N., Laitinen, T., Kulmala, M., Petäjä, T., and
Sipilä, M.: Measurement report: Long-term measurements of aerosol precursor concentrations in the Finnish subarctic boreal
forest, Atmos. Chem. Phys., 22, 2237–2254, https://doi.org/10.5194/acp-22-2237-2022, 2022.

Kalkavouras, P., BougiatiotI, A., Hussein, T., Kalivitis, N., Stavroulas, I., Michalopoulos, P., and Mihalopoulos, N.: Regional
New Particle Formation over the Eastern Mediterranean and Middle East, Atmosphere, 12, 13,
620 https://doi.org/10.3390/atmos12010013, 2020.

Kammer, J., Perraudin, E., Flaud, P.-M., Lamaud, E., Bonnefond, J. M., and Villenave, E.: Observation of nighttime new
particle formation over the French Landes forest, Science of The Total Environment, 621, 1084–1092,
https://doi.org/10.1016/j.scitotenv.2017.10.118, 2018.

Kerminen, V.-M., Chen, X., Vakkari, V., Petäjä, T., Kulmala, M., and Bianchi, F.: Atmospheric new particle formation and
625 growth: review of field observations, Environ. Res. Lett., 13, 103003, https://doi.org/10.1088/1748-9326/aadf3c, 2018.

Kodros, J. K., Papanastasiou, D. K., Paglione, M., Masiol, M., Squizzato, S., Florou, K., Skyllakou, K., Kaltsonoudis, C.,
Nenes, A., and Pandis, S. N.: Rapid dark aging of biomass burning as an overlooked source of oxidized organic aerosol, Proc.
Natl. Acad. Sci. U.S.A., 117, 33028–33033, https://doi.org/10.1073/pnas.2010365117, 2020.

Kolesar, K. R., Cellini, J., Peterson, P. K., Jefferson, A., Tuch, T., Birmili, W., Wiedensohler, A., and Pratt, K. A.: Effect of
630 Prudhoe Bay emissions on atmospheric aerosol growth events observed in Utqiaġvik (Barrow), Alaska, Atmospheric
Environment, 152, 146–155, https://doi.org/10.1016/j.atmosenv.2016.12.019, 2017.

17

Kulmala, M., Petäjä, T., Nieminen, T., Sipilä, M., Manninen, H. E., Lehtipalo, K., Dal Maso, M., Aalto, P. P., Junninen, H., Paasonen, P., Riipinen, I., Lehtinen, K. E. J., Laaksonen, A., and Kerminen, V.-M.: Measurement of the nucleation of atmospheric aerosol particles, Nat Protoc, 7, 1651–1667, https://doi.org/10.1038/nprot.2012.091, 2012.

635 Kulmala, M., Kontkanen, J., Junninen, H., Lehtipalo, K., Manninen, H. E., Nieminen, T., Petäjä, T., Sipilä, M., Schobesberger, S., Rantala, P., Franchin, A., Jokinen, T., Järvinen, E., Äijälä, M., Kangasluoma, J., Hakala, J., Aalto, P. P., Paasonen, P., Mikkilä, J., Vanhanen, J., Aalto, J., Hakola, H., Makkonen, U., Ruuskanen, T., Mauldin, R. L., Duplissy, J., Vehkamäki, H., Bäck, J., Kortelainen, A., Riipinen, I., Kurtén, T., Johnston, M. V., Smith, J. N., Ehn, M., Mentel, T. F., Lehtinen, K. E. J., Laaksonen, A., Kerminen, V.-M., and Worsnop, D. R.: Direct Observations of Atmospheric Aerosol Nucleation, Science, 339, 640 943–946, https://doi.org/10.1126/science.1227385, 2013.

Kulmala, M., Junninen, H., Dada, L., Salma, I., Weidinger, T., Thén, W., Vörösmarty, M., Komsaare, K., Stolzenburg, D., Cai, R., Yan, C., Li, X., Deng, C., Jiang, J., Petäjä, T., Nieminen, T., and Kerminen, V.-M.: Quiet New Particle Formation in the Atmosphere, Front. Environ. Sci., 10, 912385, https://doi.org/10.3389/fenvs.2022.912385, 2022.

Kürten, A.: New particle formation from sulfuric acid and ammonia: nucleation and growth model based on thermodynamics 645 derived from CLOUD measurements for a wide range of conditions, Atmos. Chem. Phys., 19, 5033–5050, https://doi.org/10.5194/acp-19-5033-2019, 2019.

Lanz, V. A., Alfarra, M. R., Baltensperger, U., Buchmann, B., Hueglin, C., and Prévôt, A. S. H.: Source apportionment of submicron organic aerosols at an urban site by factor analytical modelling of aerosol mass spectra, Atmos. Chem. Phys., 7, 1503–1522, https://doi.org/10.5194/acp-7-1503-2007, 2007.

650 Ledoux, F., Roche, C., Cazier, F., Beaugard, C., and Courcot, D.: Influence of ship emissions on NO_x, SO_2, O_3 and PM concentrations in a North-Sea harbor in France, Journal of Environmental Sciences, 71, 56–66, https://doi.org/10.1016/j.jes.2018.03.030, 2018.

Lee, S., Gordon, H., Yu, H., Lehtipalo, K., Haley, R., Li, Y., and Zhang, R.: New Particle Formation in the Atmosphere: From Molecular Clusters to Global Climate, J. Geophys. Res. Atmos., 124, 7098–7146, https://doi.org/10.1029/2018JD029356, 655 2019.

Lehtipalo, K., Yan, C., Dada, L., Bianchi, F., Xiao, M., Wagner, R., Stolzenburg, D., Ahonen, L. R., Amorim, A., Baccarini, A., Bauer, P. S., Baumgartner, B., Bergen, A., Bernhammer, A.-K., Breitenlechner, M., Brilke, S., Buchholz, A., Mazon, S. B., Chen, D., Chen, X., Dias, A., Dommen, J., Draper, D. C., Duplissy, J., Ehn, M., Finkenzeller, H., Fischer, L., Frege, C., Fuchs, C., Garmash, O., Gordon, H., Hakala, J., He, X., Heikkinen, L., Heinritzi, M., Helm, J. C., Hofbauer, V., Hoyle, C. R., 660 Jokinen, T., Kangasluoma, J., Kerminen, V.-M., Kim, C., Kirkby, J., Kontkanen, J., Kürten, A., Lawler, M. J., Mai, H., Mathot, S., Mauldin, R. L., Molteni, U., Nichman, L., Nie, W., Nieminen, T., Ojdanic, A., Onnela, A., Passananti, M., Petäjä, T., Piel, F., Pospisilova, V., Quéléver, L. L. J., Rissanen, M. P., Rose, C., Sarnela, N., Schallhart, S., Schuchmann, S., Sengupta, K., Simon, M., Sipilä, M., Tauber, C., Tomé, A., Tröstl, J., Väisänen, O., Vogel, A. L., Volkamer, R., Wagner, A. C., Wang, M., Weitz, L., Wimmer, D., Ye, P., Ylisirniö, A., Zha, Q., Carslaw, K. S., Curtius, J., Donahue, N. M., Flagan, R. C., Hansel, A., 665 Riipinen, I., Virtanen, A., Winkler, P. M., Baltensperger, U., Kulmala, M., and Worsnop, D. R.: Multicomponent new particle formation from sulfuric acid, ammonia, and biogenic vapors, Sci. Adv., 4, eaau5363, https://doi.org/10.1126/sciadv.aau5363, 2018.

Lohmann, U. and Feichter, J.: Global indirect aerosol effects: a review, Atmos. Chem. Phys., 5, 715–737, https://doi.org/10.5194/acp-5-715-2005, 2005.

670 Mahowald, N., Ward, D. S., Kloster, S., Flanner, M. G., Heald, C. L., Heavens, N. G., Hess, P. G., Lamarque, J.-F., and Chuang, P. Y.: Aerosol Impacts on Climate and Biogeochemistry, Annu. Rev. Environ. Resour., 36, 45–74, https://doi.org/10.1146/annurev-environ-042009-094507, 2011.

Marrero-Ortiz, W., Hu, M., Du, Z., Ji, Y., Wang, Y., Guo, S., Lin, Y., Gomez-Hernandez, M., Peng, J., Li, Y., Secrest, J., Zamora, M. L., Wang, Y., An, T., and Zhang, R.: Formation and Optical Properties of Brown Carbon from Small α-675 Dicarbonyls and Amines, Environ. Sci. Technol., 53, 117–126, https://doi.org/10.1021/acs.est.8b03995, 2019.

Maso, M. D., Kulmala, M., Riipinen, I., Wagner, R., Hussein, T., Aalto, P. P., and Lehtinen, K. E. J.: Formation and growth of fresh atmospheric aerosols: eight years of aerosol size distribution data from SMEAR II, Hyytiälä, Finland, Boreal Environment Research, 10, 323–336, 2005.

Mensah, A. A., Holzinger, R., Otjes, R., Trimborn, A., Mentel, Th. F., ten Brink, H., Henzing, B., and Kiendler-Scharr, A.: 680 Aerosol chemical composition at Cabauw, The Netherlands as observed in two intensive periods in May 2008 and March 2009, Atmos. Chem. Phys., 12, 4723–4742, https://doi.org/10.5194/acp-12-4723-2012, 2012.

Middlebrook, A. M., Bahreini, R., Jimenez, J. L., and Canagaratna, M. R.: Evaluation of Composition-Dependent Collection Efficiencies for the Aerodyne Aerosol Mass Spectrometer using Field Data, Aerosol Science and Technology, 46, 258–271, https://doi.org/10.1080/02786826.2011.620041, 2012.

685 Modini, R. L., Ristovski, Z. D., Johnson, G. R., He, C., Surawski, N., Morawska, L., Suni, T., and Kulmala, M.: New particle formation and growth at a remote, sub-tropical coastal location, Atmos. Chem. Phys., 9, 7607–7621, https://doi.org/10.5194/acp-9-7607-2009, 2009.

Mooibroek, D., Schaap, M., Weijers, E. P., and Hoogerbrugge, R.: Source apportionment and spatial variability of PM2.5 using measurements at five sites in the Netherlands, Atmospheric Environment, 45, 4180–4191, 690 https://doi.org/10.1016/j.atmosenv.2011.05.017, 2011.

Mordas, G., Plauškaitė, K., Prokopčiuk, N., Dudoitis, V., Bozzetti, C., and Ulevicius, V.: Observation of new particle formation on Curonian Spit located between continental Europe and Scandinavia, Journal of Aerosol Science, 97, 38–55, https://doi.org/10.1016/j.jaerosci.2016.03.002, 2016.

Németh, Z. and Salma, I.: Spatial extension of nucleating air masses in the Carpathian Basin, Atmos. Chem. Phys., 14, 8841– 695 8848, https://doi.org/10.5194/acp-14-8841-2014, 2014.

Ng, N. L., Canagaratna, M. R., Zhang, Q., Jimenez, J. L., Tian, J., Ulbrich, I. M., Kroll, J. H., Docherty, K. S., Chhabra, P. S., Bahreini, R., Murphy, S. M., Seinfeld, J. H., Hildebrandt, L., Donahue, N. M., DeCarlo, P. F., Lanz, V. A., Prévôt, A. S. H., Dinar, E., Rudich, Y., and Worsnop, D. R.: Organic aerosol components observed in Northern Hemispheric datasets from Aerosol Mass Spectrometry, Atmos. Chem. Phys., 10, 4625–4641, https://doi.org/10.5194/acp-10-4625-2010, 2010.

700 Ng, N. L., Herndon, S. C., Trimborn, A., Canagaratna, M. R., Croteau, P. L., Onasch, T. B., Sueper, D., Worsnop, D. R., Zhang, Q., Sun, Y. L., and Jayne, J. T.: An Aerosol Chemical Speciation Monitor (ACSM) for Routine Monitoring of the Composition and Mass Concentrations of Ambient Aerosol, Aerosol Science and Technology, 45, 780–794, https://doi.org/10.1080/02786826.2011.560211, 2011.

Nieminen, T., Asmi, A., Maso, M. D., Aalto, P. P., Keronen, P., Petäjä, T., Kulmala, M., and Kerminen, V.-M.: Trends in 705 atmospheric new-particle formation: 16 years of observations in a boreal-forest environment, Boreal Environment Research, 19 (suppl. B), 191–214, 2014.

Olin, M., Okuljar, M., Rissanen, M. P., Kalliokoski, J., Shen, J., Dada, L., Lampimäki, M., Wu, Y., Lohila, A., Duplissy, J., Sipilä, M., Petäjä, T., Kulmala, M., and Dal Maso, M.: Measurement report: Atmospheric new particle formation in a coastal agricultural site explained with binPMF analysis of nitrate CI-APi-TOF spectra, https://doi.org/10.5194/acp-2022-261, 22 710 April 2022.

Paatero, P.: The Multilinear Engine—A Table-Driven, Least Squares Program for Solving Multilinear Problems, Including the *n*-Way Parallel Factor Analysis Model, Journal of Computational and Graphical Statistics, 8, 854–888, https://doi.org/10.1080/10618600.1999.10474853, 1999.

Paatero, P. and Tapper, U.: Positive matrix factorization: A non-negative factor model with optimal utilization of error 715 estimates of data values, Environmetrics, 5, 111–126, https://doi.org/10.1002/env.3170050203, 1994.

Pachon, J. E., Weber, R. J., Zhang, X., Mulholland, J. A., and Russell, A. G.: Revising the use of potassium (K) in the source apportionment of PM$_{2.5}$, Atmospheric Pollution Research, 4, 14–21, https://doi.org/10.5094/APR.2013.002, 2013.

Paglione, M., Kiendler-Scharr, A., Mensah, A. A., Finessi, E., Giulianelli, L., Sandrini, S., Facchini, M. C., Fuzzi, S., Schlag, P., Piazzalunga, A., Tagliavini, E., Henzing, J. S., and Decesari, S.: Identification of humic-like substances (HULIS) in 720 oxygenated organic aerosols using NMR and AMS factor analyses and liquid chromatographic techniques, Atmos. Chem. Phys., 14, 25–45, https://doi.org/10.5194/acp-14-25-2014, 2014.

Peltola, M., Rose, C., Trueblood, J. V., Gray, S., Harvey, M., and Sellegri, K.: New particle formation in coastal New Zealand with a focus on open-ocean air masses, Atmos. Chem. Phys., 22, 6231–6254, https://doi.org/10.5194/acp-22-6231-2022, 2022.

Peng, Y., Liu, X., Dai, J., Wang, Z., Dong, Z., Dong, Y., Chen, C., Li, X., Zhao, N., and Fan, C.: Aerosol size distribution and 725 new particle formation events in the suburb of Xi'an, northwest China, Atmospheric Environment, 153, 194–205, https://doi.org/10.1016/j.atmosenv.2017.01.022, 2017.

Pio, C. A., Legrand, M., Alves, C. A., Oliveira, T., Afonso, J., Caseiro, A., Puxbaum, H., Sanchez-Ochoa, A., and Gelencsér, A.: Chemical composition of atmospheric aerosols during the 2003 summer intense forest fire period, Atmospheric Environment, 42, 7530–7543, https://doi.org/10.1016/j.atmosenv.2008.05.032, 2008.

730   Pope, C. A., Coleman, N., Pond, Z. A., and Burnett, R. T.: Fine particulate air pollution and human mortality: 25+ years of cohort studies, Environmental Research, 183, 108924, https://doi.org/10.1016/j.envres.2019.108924, 2020.

Pospisilova, V., Lopez-Hilfiker, F. D., Bell, D. M., El Haddad, I., Mohr, C., Huang, W., Heikkinen, L., Xiao, M., Dommen, J., Prevot, A. S. H., Baltensperger, U., and Slowik, J. G.: On the fate of oxygenated organic molecules in atmospheric aerosol particles, Sci. Adv., 6, eaax8922, https://doi.org/10.1126/sciadv.aax8922, 2020.

735   Pushpawela, B., Jayaratne, R., and Morawska, L.: The influence of wind speed on new particle formation events in an urban environment, Atmospheric Research, 215, 37–41, https://doi.org/10.1016/j.atmosres.2018.08.023, 2019.

Qi, X. M., Ding, A. J., Nie, W., Petäjä, T., Kerminen, V.-M., Herrmann, E., Xie, Y. N., Zheng, L. F., Manninen, H., Aalto, P., Sun, J. N., Xu, Z. N., Chi, X. G., Huang, X., Boy, M., Virkkula, A., Yang, X.-Q., Fu, C. B., and Kulmala, M.: Aerosol size distribution and new particle formation in the western Yangtze River Delta of China: 2 years of measurements at the SORPES
740   station, Atmos. Chem. Phys., 15, 12445–12464, https://doi.org/10.5194/acp-15-12445-2015, 2015.

Riccobono, F., Schobesberger, S., Scott, C. E., Dommen, J., Ortega, I. K., Rondo, L., Almeida, J., Amorim, A., Bianchi, F., Breitenlechner, M., David, A., Downard, A., Dunne, E. M., Duplissy, J., Ehrhart, S., Flagan, R. C., Franchin, A., Hansel, A., Junninen, H., Kajos, M., Keskinen, H., Kupc, A., Kürten, A., Kvashin, A. N., Laaksonen, A., Lehtipalo, K., Makhmutov, V., Mathot, S., Nieminen, T., Onnela, A., Petäjä, T., Praplan, A. P., Santos, F. D., Schallhart, S., Seinfeld, J. H., Sipilä, M.,
745   Spracklen, D. V., Stozhkov, Y., Stratmann, F., Tomé, A., Tsagkogeorgas, G., Vaattovaara, P., Viisanen, Y., Vrtala, A., Wagner, P. E., Weingartner, E., Wex, H., Wimmer, D., Carslaw, K. S., Curtius, J., Donahue, N. M., Kirkby, J., Kulmala, M., Worsnop, D. R., and Baltensperger, U.: Oxidation Products of Biogenic Emissions Contribute to Nucleation of Atmospheric Particles, Science, 344, 717–721, https://doi.org/10.1126/science.1243527, 2014.

Rose, C., Zha, Q., Dada, L., Yan, C., Lehtipalo, K., Junninen, H., Mazon, S. B., Jokinen, T., Sarnela, N., Sipilä, M., Petäjä, T.,
750   Kerminen, V.-M., Bianchi, F., and Kulmala, M.: Observations of biogenic ion-induced cluster formation in the atmosphere, Sci. Adv., 4, eaar5218, https://doi.org/10.1126/sciadv.aar5218, 2018.

Salimi, F., Crilley, L. R., Stevanovic, S., Ristovski, Z., Mazaheri, M., He, C., Johnson, G., Ayoko, G., and Morawska, L.: Insights into the growth of newly formed particles in a subtropical urban environment, Atmos. Chem. Phys., 15, 13475–13485, https://doi.org/10.5194/acp-15-13475-2015, 2015.

755   Schlag, P., Kiendler-Scharr, A., Blom, M. J., Canonaco, F., Henzing, J. S., Moerman, M., Prévôt, A. S. H., and Holzinger, R.: Aerosol source apportionment from 1-year measurements at the CESAR towerin Cabauw, the Netherlands, Atmos. Chem. Phys., 16, 8831–8847, https://doi.org/10.5194/acp-16-8831-2016, 2016.

Schobesberger, S., Junninen, H., Bianchi, F., Lönn, G., Ehn, M., Lehtipalo, K., Dommen, J., Ehrhart, S., Ortega, I. K., Franchin, A., Nieminen, T., Riccobono, F., Hutterli, M., Duplissy, J., Almeida, J., Amorim, A., Breitenlechner, M., Downard, A. J.,
760   Dunne, E. M., Flagan, R. C., Kajos, M., Keskinen, H., Kirkby, J., Kupc, A., Kürten, A., Kurtén, T., Laaksonen, A., Mathot, S., Onnela, A., Praplan, A. P., Rondo, L., Santos, F. D., Schallhart, S., Schnitzhofer, R., Sipilä, M., Tomé, A., Tsagkogeorgas, G., Vehkamäki, H., Wimmer, D., Baltensperger, U., Carslaw, K. S., Curtius, J., Hansel, A., Petäjä, T., Kulmala, M., Donahue, N. M., and Worsnop, D. R.: Molecular understanding of atmospheric particle formation from sulfuric acid and large oxidized organic molecules, Proc. Natl. Acad. Sci. U.S.A., 110, 17223–17228, https://doi.org/10.1073/pnas.1306973110, 2013.

765   Seinfeld, J. H. and Pandis, S. N.: Atmospheric chemistry and physics: from air pollution to climate change, 3rd edition., John Wiley & Sons, Hoboken, New Jersey, 1152 pp., 2016.

Sellegri, K., Rose, C., Marinoni, A., Lupi, A., Wiedensohler, A., Andrade, M., Bonasoni, P., and Laj, P.: New Particle Formation: A Review of Ground-Based Observations at Mountain Research Stations, Atmosphere, 10, 493, https://doi.org/10.3390/atmos10090493, 2019.

770   Spracklen, D. V., Carslaw, K. S., Merikanto, J., Mann, G. W., Reddington, C. L., Pickering, S., Ogren, J. A., Andrews, E., Baltensperger, U., Weingartner, E., Boy, M., Kulmala, M., Laakso, L., Lihavainen, H., Kivekäs, N., Komppula, M., Mihalopoulos, N., Kouvarakis, G., Jennings, S. G., O'Dowd, C., Birmili, W., Wiedensohler, A., Weller, R., Gras, J., Laj, P., Sellegri, K., Bonn, B., Krejci, R., Laaksonen, A., Hamed, A., Minikin, A., Harrison, R. M., Talbot, R., and Sun, J.: Explaining global surface aerosol number concentrations in terms of primary emissions and particle formation, Atmos. Chem. Phys., 10,
775   4775–4793, https://doi.org/10.5194/acp-10-4775-2010, 2010.

van der Swaluw, E., Asman, W. A. H., van Jaarsveld, H., and Hoogerbrugge, R.: Wet deposition of ammonium, nitrate and sulfate in the Netherlands over the period 1992–2008, Atmospheric Environment, 45, 3819–3826, https://doi.org/10.1016/j.atmosenv.2011.04.017, 2011.

Tröstl, J., Chuang, W. K., Gordon, H., Heinritzi, M., Yan, C., Molteni, U., Ahlm, L., Frege, C., Bianchi, F., Wagner, R., Simon,
780   M., Lehtipalo, K., Williamson, C., Craven, J. S., Duplissy, J., Adamov, A., Almeida, J., Bernhammer, A.-K., Breitenlechner,

M., Brilke, S., Dias, A., Ehrhart, S., Flagan, R. C., Franchin, A., Fuchs, C., Guida, R., Gysel, M., Hansel, A., Hoyle, C. R., Jokinen, T., Junninen, H., Kangasluoma, J., Keskinen, H., Kim, J., Krapf, M., Kürten, A., Laaksonen, A., Lawler, M., Leiminger, M., Mathot, S., Möhler, O., Nieminen, T., Onnela, A., Petäjä, T., Piel, F. M., Miettinen, P., Rissanen, M. P., Rondo, L., Sarnela, N., Schobesberger, S., Sengupta, K., Sipilä, M., Smith, J. N., Steiner, G., Tomè, A., Virtanen, A., Wagner, A. C., Weingartner, E., Wimmer, D., Winkler, P. M., Ye, P., Carslaw, K. S., Curtius, J., Dommen, J., Kirkby, J., Kulmala, M., Riipinen, I., Worsnop, D. R., Donahue, N. M., and Baltensperger, U.: The role of low-volatility organic compounds in initial particle growth in the atmosphere, Nature, 533, 527–531, https://doi.org/10.1038/nature18271, 2016.

Tsai, J.-H., Tsai, S.-M., Wang, W.-C., and Chiang, H.-L.: Water-soluble ionic species of coarse and fine particulate matter and gas precursor characteristics at urban and rural sites of central Taiwan, Environ Sci Pollut Res, 23, 16722–16737, https://doi.org/10.1007/s11356-016-6834-7, 2016.

Ulbrich, I. M., Canagaratna, M. R., Zhang, Q., Worsnop, D. R., and Jimenez, J. L.: Interpretation of organic components from Positive Matrix Factorization of aerosol mass spectrometric data, Atmos. Chem. Phys., 9, 2891–2918, https://doi.org/10.5194/acp-9-2891-2009, 2009.

Urban, R. C., Lima-Souza, M., Caetano-Silva, L., Queiroz, M. E. C., Nogueira, R. F. P., Allen, A. G., Cardoso, A. A., Held, G., and Campos, M. L. A. M.: Use of levoglucosan, potassium, and water-soluble organic carbon to characterize the origins of biomass-burning aerosols, Atmospheric Environment, 61, 562–569, https://doi.org/10.1016/j.atmosenv.2012.07.082, 2012.

Vehkamäki, H. and Riipinen, I.: Thermodynamics and kinetics of atmospheric aerosol particle formation and growth, Chem. Soc. Rev., 41, 5160, https://doi.org/10.1039/c2cs00002d, 2012.

Wagner, R., Yan, C., Lehtipalo, K., Duplissy, J., Nieminen, T., Kangasluoma, J., Ahonen, L. R., Dada, L., Kontkanen, J., Manninen, H. E., Dias, A., Amorim, A., Bauer, P. S., Bergen, A., Bernhammer, A.-K., Bianchi, F., Brilke, S., Mazon, S. B., Chen, X., Draper, D. C., Fischer, L., Frege, C., Fuchs, C., Garmash, O., Gordon, H., Hakala, J., Heikkinen, L., Heinritzi, M., Hofbauer, V., Hoyle, C. R., Kirkby, J., Kürten, A., Kvashnin, A. N., Laurila, T., Lawler, M. J., Mai, H., Makhmutov, V., Mauldin III, R. L., Molteni, U., Nichman, L., Nie, W., Ojdanic, A., Onnela, A., Piel, F., Quéléver, L. L. J., Rissanen, M. P., Sarnela, N., Schallhart, S., Sengupta, K., Simon, M., Stolzenburg, D., Stozhkov, Y., Tröstl, J., Viisanen, Y., Vogel, A. L., Wagner, A. C., Xiao, M., Ye, P., Baltensperger, U., Curtius, J., Donahue, N. M., Flagan, R. C., Gallagher, M., Hansel, A., Smith, J. N., Tomé, A., Winkler, P. M., Worsnop, D., Ehn, M., Sipilä, M., Kerminen, V.-M., Petäjä, T., and Kulmala, M.: The role of ions in new particle formation in the CLOUD chamber, Atmos. Chem. Phys., 17, 15181–15197, https://doi.org/10.5194/acp-17-15181-2017, 2017.

Wamelink, G. W. W., de Knegt, B., Pouwels, R., Schuiling, C., Wegman, R. M. A., Schmidt, A. M., van Dobben, H. F., and Sanders, M. E.: Considerable environmental bottlenecks for species listed in the Habitats and Birds Directives in the Netherlands, Biological Conservation, 165, 43–53, https://doi.org/10.1016/j.biocon.2013.05.012, 2013.

Wehner, B., Werner, F., Ditas, F., Shaw, R. A., Kulmala, M., and Siebert, H.: Observations of new particle formation in enhanced UV irradiance zones near cumulus clouds, Atmos. Chem. Phys., 15, 11701–11711, https://doi.org/10.5194/acp-15-11701-2015, 2015.

Wiedensohler, A., Wiesner, A., Weinhold, K., Birmili, W., Hermann, M., Merkel, M., Müller, T., Pfeifer, S., Schmidt, A., Tuch, T., Velarde, F., Quincey, P., Seeger, S., and Nowak, A.: Mobility particle size spectrometers: Calibration procedures and measurement uncertainties, Aerosol Science and Technology, 52, 146–164, https://doi.org/10.1080/02786826.2017.1387229, 2018.

Wong, J. P. S., Nenes, A., and Weber, R. J.: Changes in Light Absorptivity of Molecular Weight Separated Brown Carbon Due to Photolytic Aging, Environ. Sci. Technol., 51, 8414–8421, https://doi.org/10.1021/acs.est.7b01739, 2017.

Xing, J., Wang, J., Mathur, R., Wang, S., Sarwar, G., Pleim, J., Hogrefe, C., Zhang, Y., Jiang, J., Wong, D. C., and Hao, J.: Impacts of aerosol direct effects on tropospheric ozone through changes in atmospheric dynamics and photolysis rates, Atmos. Chem. Phys., 17, 9869–9883, https://doi.org/10.5194/acp-17-9869-2017, 2017.

Zhang, Q., Jimenez, J. L., Canagaratna, M. R., Ulbrich, I. M., Ng, N. L., Worsnop, D. R., and Sun, Y.: Understanding atmospheric organic aerosols via factor analysis of aerosol mass spectrometry: a review, Anal Bioanal Chem, 401, 3045–3067, https://doi.org/10.1007/s00216-011-5355-y, 2011.

Zhang, R., Khalizov, A., Wang, L., Hu, M., and Xu, W.: Nucleation and Growth of Nanoparticles in the Atmosphere, Chem. Rev., 112, 1957–2011, https://doi.org/10.1021/cr2001756, 2012.

Zhang, X., McVay, R. C., Huang, D. D., Dalleska, N. F., Aumont, B., Flagan, R. C., and Seinfeld, J. H.: Formation and evolution of molecular products in α-pinene secondary organic aerosol, Proc. Natl. Acad. Sci. U.S.A., 112, 14168–14173, https://doi.org/10.1073/pnas.1517742112, 2015.

Zhao, D., Pullinen, I., Fuchs, H., Schrade, S., Wu, R., Acir, I.-H., Tillmann, R., Rohrer, F., Wildt, J., Guo, Y., Kiendler-Scharr, A., Wahner, A., Kang, S., Vereecken, L., and Mentel, T. F.: Highly oxygenated organic molecule (HOM) formation in the isoprene oxidation by NO_3 radical, Atmos. Chem. Phys., 21, 9681–9704, https://doi.org/10.5194/acp-21-9681-2021, 2021.

835   Zheng, Y., Cheng, X., Liao, K., Li, Y., Li, Y. J., Huang, R.-J., Hu, W., Liu, Y., Zhu, T., Chen, S., Zeng, L., Worsnop, D. R., and Chen, Q.: Characterization of anthropogenic organic aerosols by TOF-ACSM with the new capture vaporizer, Atmos. Meas. Tech., 13, 2457–2472, https://doi.org/10.5194/amt-13-2457-2020, 2020.